Desalination and Water Treatment
www.deswater.com

doi: 10.5004/dwt.2021.27205

224 (2021) 228–242
June

Photocatalytic ozonation of municipal wastewater for degradation of phenol using Fe doped TiO_2 nanoparticles: optimization using RSM

Chhaya V. Rekhate*, J.K. Srivastava

Department of Chemical Engineering, Ujjain Engineering College, Ujjain 456006, India, Tel. +91-7389944098; emails: chhayaprafulla@gmail.com (C.V. Rekhate), profjksrivatava@gmail.com (J.K. Srivastava)

Received 26 September 2020; Accepted 22 February 2021

ABSTRACT

Photocatalytic ozonation using Fe-doped titanium dioxide nanoparticles (FeT) prepared by the molten salt method was investigated for the degradation of phenol in synthetic solution and real secondary municipal wastewater. Photocatalytic ozonation using UV radiation (UV/FeT/O_3) and solar radiation (solar/FeT/O_3) were compared and optimized using response surface methodology (RSM). The ozone dose, initial pH, catalyst concentration, reaction time, and phenol degradation efficiency as process response were explored to build up a mathematical correlation using the central composite design of RSM. The regression model was tested for statistical significance using analysis of variance. The high value of the coefficient of determination (R^2 = 0.9837 for UV/FeT/O_3 and R^2 = 0.9637 for solar/FeT/O_3) shows that the model was statistically significant showing an excellent correlation between the experimental and predicted value of phenol degradation efficiency. The RSM predicted phenol degradation efficiency of 95.73% for UV/FeT/O_3 and 86.46% for solar/FeT/O_3 obtained under optimized condition (ozone concentration = 70 mg/L; pH = 10; catalyst concentration = 0.5 g/L; reaction time = 20 min) was comparable with the experimental result. Synergy index values of 1.02–1.25 were observed between ozonation and photocatalysis using solar and UV photocatalytic ozonation.

Keywords: Ozonation; Photocatalytic oxidation; Phenol degradation; Secondary municipal wastewater; Fe doped TiO_2; Photocatalytic ozonation

1. Introduction

Due to global water scarcity, there is an increasing demand for wastewater reuse for direct human consumption. Advanced oxidation process (AOP) such as photocatalysis and ozonation has several advantages in water treatment. Owing to the low oxidation rate photocatalysis is a relatively slow process whereas ozonation results in partial oxidation of organic compounds [1]. Ozone is a selective oxidant [2]. Ozonation alone has limitations such as high energy consumption, low efficiency due to limited mass transfer [3]. Furthermore, single ozonation does not provide a satisfactory degree of elimination of TOC, toxicity, and phenol mineralization [4]. The degradation and TOC removal rate for photocatalysis combined with the ozonation process is found to be higher and complete mineralization to carbon dioxide and water can be achieved [5]. Photocatalytic ozonation is cost-efficient than ozonation and photocatalysis [6].

Many industries use phenolic material in their manufacturing processes. Phenol is used in the manufacture of paints, dyes, pharmaceuticals, pesticides, synthetic rubber, textile, weedicides, etc. The wastewater containing phenolic compounds are characterized by high chemical oxygen demand (COD) value and low biodegradability index, thus cannot be treated by the conventional aeration process. The utilization of phenol-contaminated water has severe health effects on humans and could result in severe pain causing damage to the capillaries which may lead to death [7]. Therefore, the elimination of phenol and its compounds is essential to facilitate wastewater reuse potential. The wet

* Corresponding author.

air oxidation, Fenton process, electrochemical oxidation, and ozonation are some of the methods for the removal of phenol [8,9].

TiO_2 has been the extensively used semiconductor photocatalyst due to its large bandgap, high chemical stability, low cost, and non-toxicity [10–12]. TiO_2 requires UV light for activation as it has wide bandgap (3.2 eV) [13]. Many methods have been used to improve the visible light activity of TiO_2-based photocatalysts such as doping with metal ions like Ag, Cu, Fe, etc., [14] and by using composite semiconductors such as NiO/TiO_2 [15]. A high-energy ball milling process could be an alternative for preparing nano-sized particles [16].

In the present study, Fe doping has been explored. The ionic radius of Fe^{3+} (0.64 Å) is almost the same as that of Ti^{4+} (0.68 A°) as a result Fe^{3+} can be easily integrated into the TiO_2 matrix [17,18]. Fe doped TiO_2 material shows *n*-type semiconducting behavior [19]. The phase transformation into the anatase phase occurs upon Fe-doping [20]. Fe^{3+} ions inhibit the recombination of photogenerated electron–hole pair by acting as charge carrier trap thereby, increasing photo activity [10,21]. The photocatalytic activities of Fe-doped TiO_2 nanocatalyst (FeT) were found to be about 2.5 times higher than pure TiO_2 [22]. Further solar photocatalytic ozonation processes can be cheaper than the solar photo-Fenton system [23].

Photocatalytic ozonation processes are less ozone-consuming technologies [24]. The synergistic effect of photocatalytic ozonation in the degradation of organic pollutants results due to the reduction of photogenerated electron–hole recombination on the surface of TiO_2 as Fe^{3+} ions can act as electron and hole trapping sites [25], and generation of powerful hydroxyl ($OH^{\bullet}$) radicals produced by ozone enhance the oxidation rates [26]. It was observed that there was no bacterial re-growth after UV and solar photocatalytic ozonation since bacterial cells were irreparably damaged [27]. Mecha et al. [28] analyzed the cytotoxicity of the wastewater and observed that water treated by photocatalytic ozonation was less toxic.

The photocatalytic ozonation takes place through a chain of complex reactions. The $OH^{\bullet}$ radicals are produced on the TiO_2 surface through the formation of $O_3^{\bullet-}$ radicals in a series of steps [25]. Fig. 1 demonstrates the photocatalytic ozonation reaction mechanism. The photogenerated holes and electrons produced when light falls on the surface of FeT photocatalyst, participated in the redox reactions resulting in the generation of superoxide radical anion ($O_2^{\bullet-}$) and hydroxyl radical ($OH^{\bullet}$), respectively, as illustrated by Eqs. (1)–(12):

$$FeT + h\gamma \rightarrow h^+ + e^- \quad (1)$$

$$O_3 + e^- \rightarrow O_3^{\bullet-} \quad (2)$$

$$O_3^{\bullet-} + H^+ \rightarrow HO_3^{\bullet} \quad (3)$$

$$HO_3^{\bullet} \rightarrow O_2 + OH^{\bullet} \quad (4)$$

$$H_2O_2 \rightarrow HO_2^- + H^+ \quad (5)$$

$$Fe^{3+} + e^- \rightarrow Fe^{2+} \quad (6)$$

$$Fe^{3+} + h^- \rightarrow Fe^{4+} \quad (7)$$

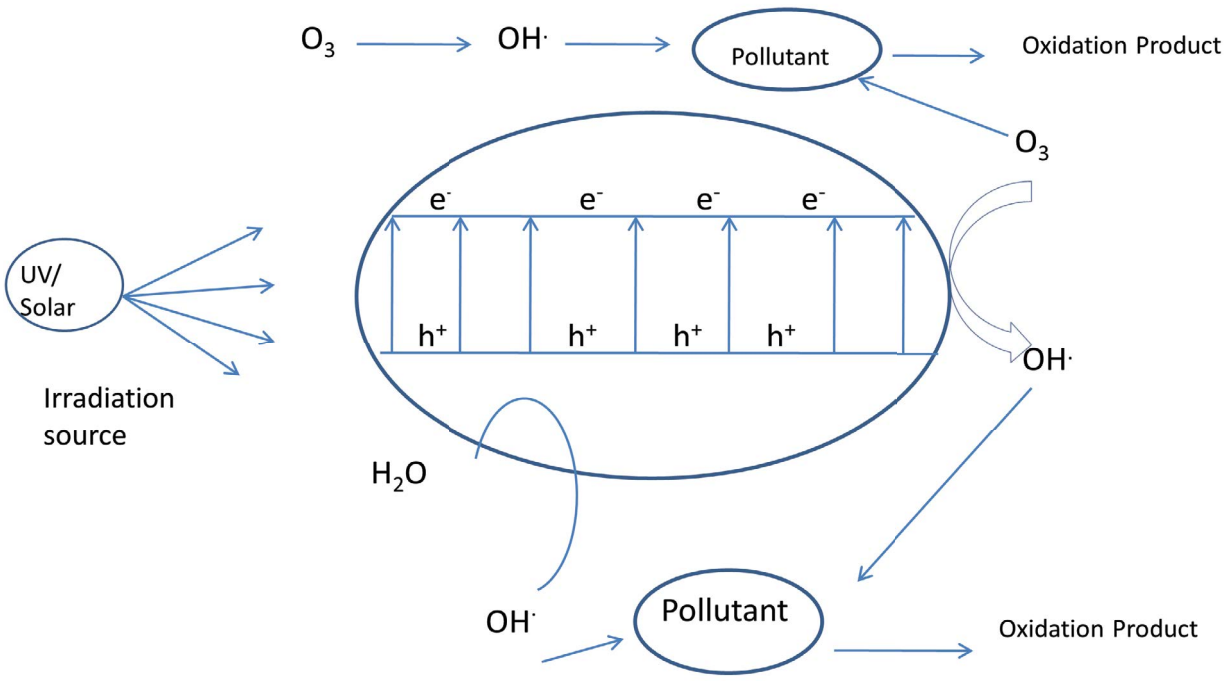

Fig. 1. Reaction mechanism of photocatalytic ozonation.

$$Fe^{4+} + OH^- \rightarrow Fe^{3+} + OH^\bullet \quad (8)$$

Since the formation of H_2O_2 during phenol ozonation is expected, homogeneous/heterogeneous (photo) Fenton reactions could develop.

$$H_2O_2 + Fe^{3+} \rightarrow Fe^{3+} + OH^- + OH^\bullet \quad (9)$$

$$Fe^{3+} + H_2O + h\gamma \rightarrow OH^\bullet + Fe^{3+} + H^+ \quad (10)$$

The synergy effect of photocatalytic and ozonation is developed by competent trapping of photogenerated electrons by ozone [25].

$$e^- + O_2 \rightarrow O_2^{\bullet -} \quad (11)$$

$$O_2^{\bullet -} + O_3 \rightarrow O_3^{\bullet -} + O_2 \quad (12)$$

More ever the utilization of natural sunlight rather than energy-intensive commercial UV lamp was employed in the present study to develop cost-effective wastewater treatment technologies. There are few reports of photocatalytic ozonation using solar light active photocatalyst. Also, most studies have been carried out in synthetic water using only one organic pollutant. The study involving real secondary municipal wastewater which contains a complicated water matrix is essential to extend processes for practical application. The present study explored the photocatalytic ozonation using UV and solar light for the treatment of synthetic water and secondary municipal wastewater containing phenol using FeT nanocatalyst prepared by the molten salt method. The novelty of the work is that such a catalyst is used for the first time in photocatalytic ozonation for municipal wastewater treatment. Response surface methodology (RSM) was employed to optimize process parameters like ozone dose, initial pH, catalyst concentration, reaction time, and phenol degradation efficiency as process response.

The objective of the present study is (a) to study the effectiveness of FeT nanocatalyst for the degradation of phenol using photocatalytic ozonation of synthetic phenol solution and secondary municipal wastewater; (b) to optimize the process parameter like ozone concentration, initial pH, catalyst concentration, and reaction time using RSM; (c) to determine synergy index; (d) to determine reaction rate constants.

2. Materials and methods

$FeCl_3$ and titanium dioxide powder were procured from Merck Company (Germany). Fe doped TiO_2 (FeT) was synthesized as explained in previous work [29]. Briefly, 0.03 g of $FeCl_3$ equivalent to 3 wt.% of iron chloride was taken to a Petri dish and 1–2 drops of deionized water were added to dissolve iron chloride. Then 1 g of pure TiO_2 was added to it. The mixture is grinded and stirred continuously for about 1 h so that iron chloride uniformly spread in the mixture, the sample was placed in a furnace at a constant temperature of 700°C ± 5°C for 1 h. The sample was removed from the furnace and then dried at ambient temperature. Potassium iodide (KI), sodium thiosulphate, starch, potassium dichromate, phenol (95%), sulfuric acid, and NaOH were of analytical grade. An ozone generator (model S1-300, A. M. Ozonics, Mumbai) was used for the generation of ozone using pure oxygen supplied by a medicinal-grade oxygen cylinder. For UV radiation two UVA lamp (11 W, 365 nm, Philips), India was used. The intensity of UV-vis radiation was 20 mW cm^{-1}.

2.1. Characterization of photocatalyst

SEM image of FeT nanoparticles is presented in Fig. 2. The SEM image indicated the spherical shape of FeT nanoparticles. The XRD pattern of FeT nanoparticles is shown in Fig. 3. The average crystalline size of FeT nanoparticles estimated using the Scherrer equation [29] was about 44.2 nm in diameter. The photocatalyst displayed a crystalline nature with peaks for anatase and rutile as the mixed-phase. 2θ peaks in XRD pattern of prepared FeT catalyst was consistent with anatase (101), (004), (200), (211), (204), (116), and (220) lattice planes (JCP DS No. 21-1272). The diffraction peaks corresponding to the rutile phase (121) and (111) lattice planes (JCP DS No. 21-1276) are also observed.

Fig. 4a shows the UV-vis reflectance spectra of the Fe doped TiO_2 nanoparticles. It was well-known that increased absorption at a wavelength less than 380 nm is associated with bandgap (about 3.2 eV) absorption of pure anatase TiO_2, Fe doping results in absorption in the visible region.

Kubelka–Munk extrapolation plot was used to evaluate the bandgap of nanoparticles. The line drawn on the linear part of the plot of $(h\nu\alpha)^{0.5}$ vs. hν gives bandgap [30]. It was observed that (Fig. 4b) the bandgap energy for 3%Fe doped TiO_2 is ~2.8 eV with a redshift that leads to successful utilization of solar energy, which is comparable to the bandgap of Fe doped TiO_2 in similar studies [14,21].

2.2. Characterization of wastewater

Synthetic water and actual municipal secondary wastewater (SWW) obtained from the Kabitkhedi sewage treatment plant in Indore, India was used in this study. The samples were collected after the biological treatment stage and analyzed in the laboratory for physicochemical parameters within 24 h using standard methods. The characteristics

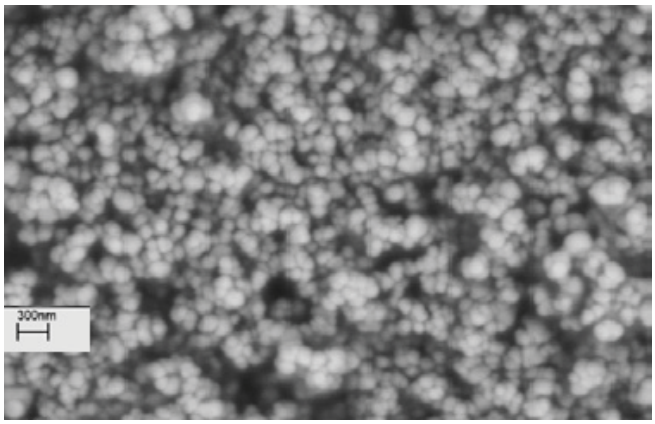

Fig. 2. SEM images of TiO_2 nanoparticles doped with 3% Fe.

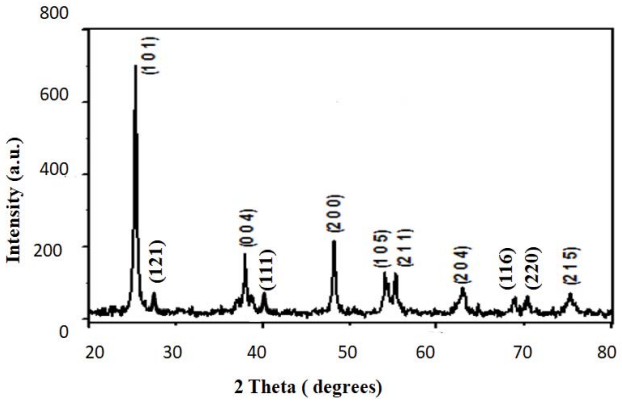

Fig. 3. XRD pattern of TiO_2 nanoparticles doped with 3% Fe.

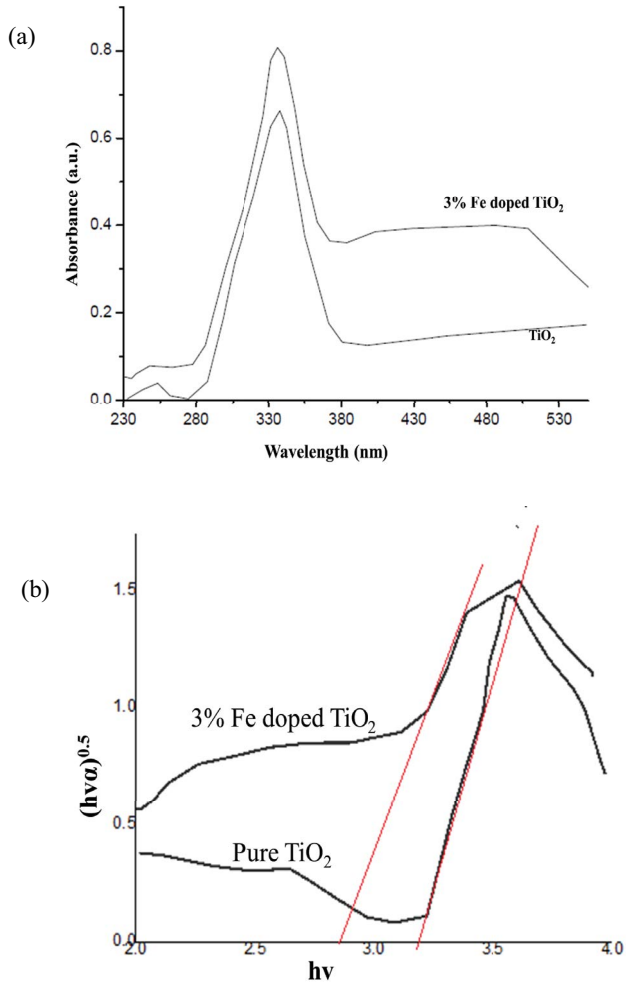

Fig. 4. (a) UV/vis reflectance spectra of Fe doped TiO_2 nanoparticles and (b) band gap of pure TiO_2 and Fe doped TiO_2 nanoparticles.

of SWW are mentioned in Table 1. The stock solution of synthetic phenol water was made by spiking deionized water with phenol. The typical phenol concentration in municipal wastewater may vary from 500 to 5,000 μg L^{-1}. The phenol solution (1 L) of concentration 500 mg L^{-1} was chosen to determine the robustness of the treatment process for all RSM experiments and to facilitate the investigation of chemical reaction kinetics. Further many articles explored phenol concentration up to 100 mg L^{-1} and phenol concentration up to 500 mg L^{-1} is explored by very few.

Table 1
Characteristics of the secondary municipal effluent (SWW)

Parameter	pH	Turbidity (NTU)	COD	BOD_5 (mg L^{-1})	Phenol (mg L^{-1})
Value	7.3	1[a]	44	35	500[b]

[a]Water samples were filtered using a Whatman filter paper.
[b]spiked.

2.3. Experimental setup and analysis

Experiments were carried out in a cylindrical glass reactor (1 L). Figs. 5a and b illustrate the experimental setup for photocatalytic ozonation using UV radiation (UV/FeT/O_3) and solar radiation (solar/FeT/O_3), respectively. The ozone is bubbled continuously into the reactor using a pipe diffuser. The magnetic stirrer keeps the catalyst in suspension. The FeT catalyst was not added and the UV lamp was switched off with a continuous supply of ozone during ozonation while during photocatalysis, the UV lamp was switched on, FeT catalyst was added with no ozone supply. The UV/FeT/O_3 process was conducted with a continuous supply of ozone in the presence of FeT catalyst and with a UV lamp switched on. Ozone in the gas leaving the reactor was measured to calculate the ozone consumed. During solar/FeT/O_3, the glass reactor (1 m in length and 0.05 m in diameter) was used together with an aluminum solar parabolic collector and was exposed to solar radiation by conducting experiments on sunny days between 11:00 a.m. to 03:00 p.m. local time and manual tracking was used to orient the reactor to the incident solar radiation. Prior to irradiation, the feed was stirred in the dark for 30 min to establish adsorption–desorption equilibrium in the feed tank, thereafter it was pumped to the reactor exposed to UV/solar light.

The ozone concentration in the feed gas was measured by the Iodometric standard method. 1 M H_2SO_4 and NaOH were used to adjust pH and were determined by a digital pH meter. COD was determined by the COD analyzer using the standard method. The 5 d biochemical oxygen demand (BOD_5) test was used to measure biodegradability. Turbidity was measured using a digital turbidity meter. The samples were taken at a specific time interval to analyze phenol degradation efficiency. Phenol concentration (at 270 nm) was determined using a UV-vis spectrophotometer (Shimadzu UV-1800, Japan) after filtration of the samples using 0.45 μm filter papers. The phenol degradation efficiency after photocatalytic ozonation treatment was calculated using Eq. (13):

$$R = \left(\frac{C_0 - C_t}{C_0}\right) \times 100 \quad (13)$$

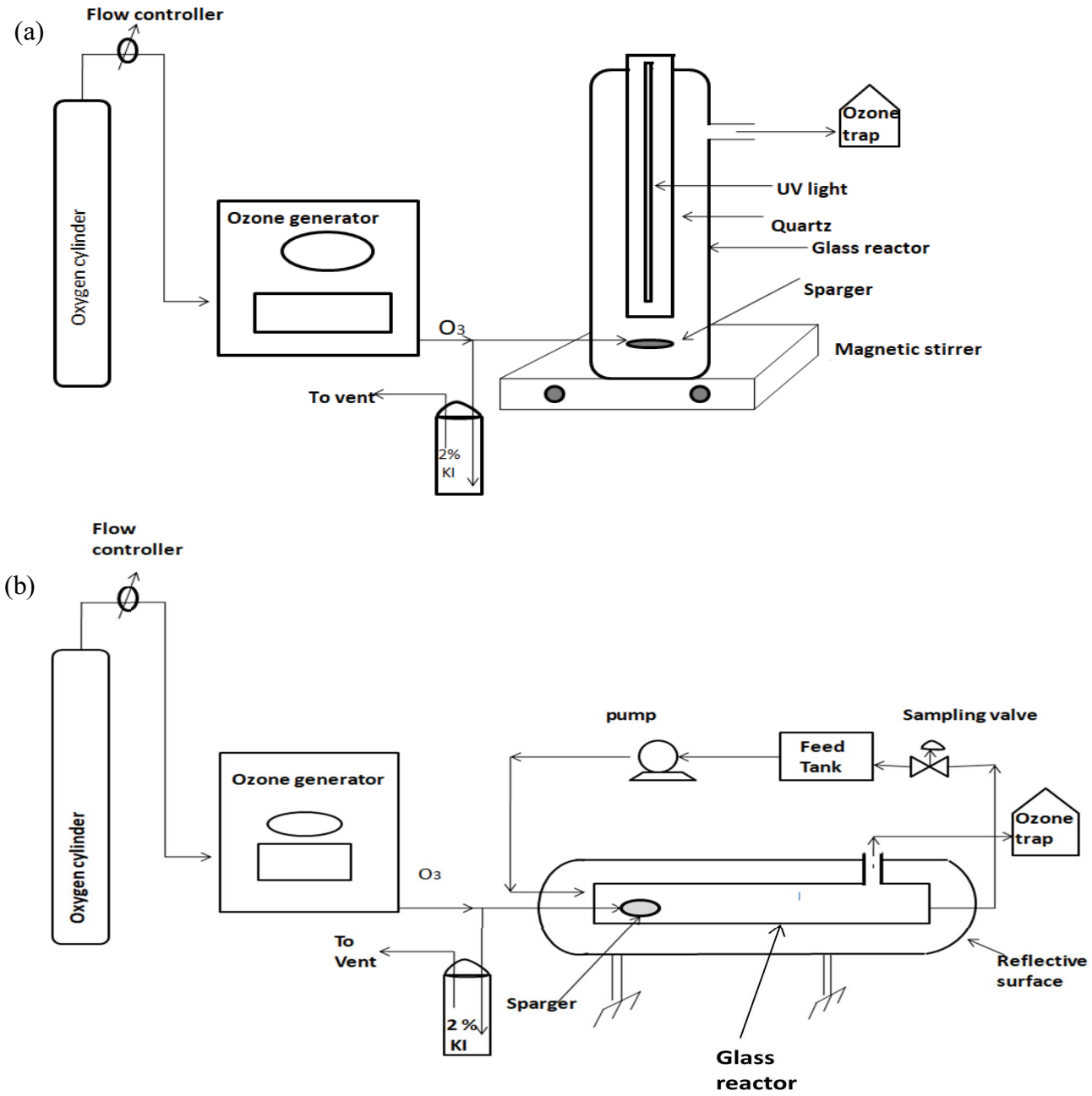

Fig. 5. Experimental setup for: (a) UV/FeT/O_3 and (b) solar/FeT/O_3 process.

where R is percentage phenol degradation efficiency, C_0 (mg L^{-1}) is initial phenol concentration, and C_t (mg L^{-1}) is the concentration at time t (min).

2.4. Design of experiment and RSM modeling

Central composite design (CCD) which is a commonly used form of response surface methodology was employed. The influence of reaction conditions on phenol degradation efficiency was determined using four independent factors: initial ozone concentration (X_1), initial pH of the solution (X_2), catalyst concentration (X_3), and reaction time (X_4). The experiments were done for photocatalytic ozonation using UV light and solar radiation. A total of 30 experiments were done for each AOP including 2^4 = 16 cube points, 2 × 4 = 8 axial points with six replications at the center points. The process variable and their actual and coded levels used for RSM are shown in Table 2. The statistical analysis of experimental data was done using Design Expert 12. Table 3 represents the parameter setting for RSM modeling. The experimental data were then fitted with a second-order polynomial equation [Eq. (14)] to correlate the response variable to the independent variable.

Table 2
Process variables and their actual and coded levels used for RSM

Independent parameter	Coded variable	Actual values of coded variable and level				
		–2	–1	0	1	2
Ozone concentration (mg L^{-1})	X_1	25	40	55	70	85
Initial pH	X_2	1	4	7	10	13
Catalyst concentration (g L^{-1})	X_2	0.25	0.5	0.75	1.0	1.25
Reaction time (min)	X_4	5	10	15	20	25

Table 3
RSM parameter

RSM	
Parameter	Value
Input variable	4
Output variable	1
Run	30
Initial design	Central composite
Design mode	Quadratic
Block	No block

$$Y = B_0 + \sum_{i=1}^{n} B_i X_i + \sum_{i=1}^{n-1} B_{ii} X_i^2 + \sum_{i=1}^{n-1} \sum_{j=i+1}^{n} B_{ij} X_i X_j + \varepsilon \quad (14)$$

where Y is phenol degradation efficiency, B_0, B_i, B_{ii}, and B_{ij} are the regression constants for intercept, linear, quadratic, and interaction coefficients, respectively, n is the number of variables studied. X_i and X_j are input variables and ε is a random error. The regression mathematical model was tested for statistical significance using analysis of variance (ANOVA). ANOVA compares variation due to residual with a variance of data about mean *F*-test [31].

3. Result and discussion

The experiments using CCD were performed to explore the effect of the independent variable on phenol degradation efficiency. Table 4 represents the four-factor full factorial CCD matrix, experimental, and predicted phenol degradation efficiency for UV and solar photocatalytic ozonation. ANOVA results presented in Tables 5a and b were employed to assess the model. A small *p*-value showed that the quadratic model developed was statistically significant and could be used to predict phenol degradation efficiency. The higher value of the coefficient of determination (R^2 = 0.9837 for UV and R^2 = 0.9637 for solar photocatalytic ozonation) showed that the model was statistically significant indicating a good correlation between observed and predicted values of the response. The values of the adjusted determination coefficients (adjusted R^2 = 0.9685 for UV/FeT/O_3; 0.9299 for solar/FeT/O_3 process) indicated that 96.85%, and 92.99% of total variations for UV/FeT/O_3, and solar/FeT/O_3 process, respectively, were explained by the developed RSM model. The coefficients for the second-order polynomial model in terms of coded and actual factors are given in Table 6. The plot between experimental and predicted degradation efficiency (Fig. 6) indicated a good correlation between model-predicted and observed values. Fig. 7 represents the distribution of residuals for RSM. The sum of square (SS) of each source quantifies its importance in the degradation process, as the value of SS increases the significance of the corresponding source also increases [32]. It was observed that pH and time were the most influential variables. The effects of square terms were found to be negligible compared to other terms. The interactions between pH and time were significant while the interaction between other variable has no effect on phenol degradation.

3.1. Effect of initial pH

As it is well-known, one of the advantages of the usage of ozone in water treatment is its selectivity toward different structures, double C–C bonds, and phenolics among them. Thus, in the case of phenol, the second-order rate constant of its reaction with ozone is high and increases with pH due to the higher reactivity of the phenolate [33]. Contrary to O_3, $OH^{\bullet}$ radicals are non-selective species that react extremely fast with most organics and enhance the degradation of refractory organics. Decomposition of O_3 into $OH^{\bullet}$ could be promoted in presence of UV, H_2O_2, catalysts, etc. [34]. An increase in the pH (i.e., a higher concentration of hydroxide anion) also promoted this decomposition [33].

Fig. 8 represents response surfaces for UV/FeT/O_3, and solar/FeT/O_3 processes as a function of initial pH and reaction time. Fig. 9 represents response surfaces for UV/FeT/O_3, and solar/FeT/O_3 processes as a function of catalyst concentration and initial pH. The pH was adjusted initially and as the oxidation proceeds, a decrease in pH was expected due to the generation of acidic intermediates. The photocatalytic degradation involved radical oxidation, direct electron transfer, and surface sorption reaction [13].

It was observed that under acidic conditions, the phenol degradation efficiency was higher and increased with increasing pH until pH 10 and then decreased quickly. This could imply that the affinity between phenol and FeT enhanced in acidic conditions. The lower activity at alkaline pH may be due to competition between phenoxide ions ($C_6H_5O^-$) and OH^- for limited reactive sites on the photocatalyst leading to a reduction in generation of $OH^{\bullet}$ radical due to fewer active sites available for $OH^{\bullet}$ generation. It has been observed that ozone transfer efficiency decreases at high pH as the increase in reaction rate is counterbalanced by greater ozone requirement due to loss of oxidant by self decomposition [35].

Table 4
Full factorial CCD matrix and experimental and RSM predicted phenol degradation efficiency

Run	Ozone concentration (mg L^{-1})	Initial pH	Catalyst concentration (g L^{-1})	Reaction time (min)	Experimental degradation efficiency		RSM predicted efficiency	
					UV/FeT/O_3	Solar/FeT/O_3	UV/FeT/O_3	Solar/FeT/O_3
1	40(–1)	4(–1)	0.5(–1)	10(–1)	94.19	83.19	94.14	82.56
2	70(+1)	4(–1)	0.5(–1)	10(–1)	94.89	84.89	94.21	83.41
3	40(–1)	10(+1)	0.5(+1)	10(–1)	85.90	73.96	85.15	72.98
4	70(+1)	10(+1)	0.5(+1)	10(–1)	84.71	74.71	84.87	74.67
5	55(0)	7(0)	0.75(0)	15(0)	91.24	81.24	91.19	81.41
6	40(–1)	4(–1)	1.0(+1)	10(–1)	93.68	83.68	93.51	83.10
7	70(+1)	4(–1)	1.0(+1)	10(–1)	93.19	83.19	94.03	83.12
8	40(–1)	10(+1)	1.0(+1)	10(–1)	83.26	73.26	83.92	72.81
9	70(+1)	10(+1)	1.0(+1)	10(–1)	84.78	74.78	84.10	73.67
10	55(0)	7(0)	0.75(0)	15(0)	91.59	82.59	91.19	81.41
11	40(–1)	4(–1)	0.5(–1)	20(+1)	93.52	83.72	93.63	84.59
12	70(+1)	4(–1)	0.5(–1)	20(+1)	94.52	84.92	94.35	84.91
13	40(–1)	10(+1)	0.5(+1)	20(+1)	95.69	85.69	95.34	85.30
14	70(+1)	10(+1)	0.5(+1)	20(+1)	96.12	86.12	95.72	86.46
15	55(0)	7(0)	0.75(0)	15(0)	90.56	80.56	91.19	81.41
16	40(–1)	4(–1)	1.0(+1)	20(+1)	93.23	86.23	93.56	85.81
17	70(+1)	4(–1)	1.0(+1)	20(+1)	94.57	84.57	94.75	85.31
18	40(–1)	10(+1)	1.0(+1)	20(+1)	94.58	84.58	94.69	85.82
19	70(+1)	10(+1)	1.0(+1)	20(+1)	94.98	85.98	95.52	86.15
20	55(0)	7(0)	0.75(0)	15(0)	91.64	81.64	91.19	81.41
21	25(–2)	7(0)	0.75(0)	15(0)	91.76	80.76	91.77	81.08
22	85(+2)	7(0)	0.75(0)	15(0)	92.62	81.88	92.68	82.26
23	55(0)	1(–2)	0.75(0)	15(0)	95.99	85.79	95.75	86.23
24	55(0)	13(+2)	0.75(0)	15(0)	87.23	77.23	87.54	77.49
25	55(0)	7(0)	0.25(–2)	15(0)	91.52	81.52	92.54	82.33
26	55(0)	7(0)	1.25(+2)	15(0)	92.65	82.65	91.70	82.55
27	55(0)	7(0)	300(0)	5(–2)	86.14	72.12	86.43	74.44
28	55(0)	7(0)	300(0)	25(+2)	97.56	90.56	97.34	88.94
29	55(0)	7(0)	0.75(0)	15(0)	90.77	80.77	91.19	81.41
30	55(0)	7(0)	0.75(0)	15(0)	91.36	81.63	91.19	81.41

3.2. Effect of ozone concentration

A suitable ozone flow rate for the degradation of target pollutants is required for the optimization of ozone utilization. Higher ozone concentration led to the increased driving force for the ozone mass transfer resulting in more absorption of ozone which reacts with the radical initiator (Fe^{2+}, $OH^{\bullet}$, etc.) to yield more hydroxyl radicals for phenol degradation [36]. The response surfaces showing the effect of catalyst and ozone dosage on the degradation of phenol are represented in Fig. 10. It was observed that the effect of ozone dosage on phenol degradation efficiency was not much noteworthy. It was observed that the time required for total phenol degradation decreased as ozone concentration increased.

3.3. Effect of catalyst concentration

Fig. 11 shows the response surfaces for UV/FeT/O_3 and solar/FeT/O_3 processes as a function of catalyst concentration and reaction time. The effect of catalyst concentration on photocatalytic activity was studied by varying the catalyst concentration from 0.25 to 1.25 g L^{-1}. It was observed from Figs. 9 and 10 that phenol degradation efficiency increased with catalyst loading until 0.5 g L^{-1} and thereafter decreased at high loading values. The increase in catalyst concentration might have increased the number of reactive sites thereby enhanced the light absorption for photocatalysis [14]. The higher concentrations of the photocatalyst may result in light-scattering and screening effects due to high opacity caused by an excess catalyst which

Table 5a
Analysis of variance for the fit of phenol degradation efficiency for UV/FeT/O_3, solar/FeT/O_3 processes using CCD-RSM model

Source	UV/FeT/O_3					Solar/FeT/O_3				
	Sum of squares	df	Mean square	*F*-value	*p*-value	Sum of squares	df	Mean square	*F*-value	*p*-value
Model	401.38	14	28.67	64.71	<0.0001 significant	542.89	14	38.78	28.47	<0.0001 significant
X_1-Ozone concentration	1.23	1	1.23	2.77	0.1166	2.09	1	2.09	1.54	0.234
X_2-pH	101.23	1	101.23	228.49	<0.0001	114.54	1	114.54	84.08	<0.0001
X_3-Catalyst concentration	1.05	1	1.05	2.36	0.1453	0.0737	1	0.0737	0.0541	0.8192
X_4-Reaction time	178.49	1	178.49	402.87	<0.0001	315.59	1	315.59	231.68	<0.0001
X_1X_2	0.1208	1	0.1208	0.2726	0.6092	0.7014	1	0.7014	0.5149	0.484
X_1X_3	0.2093	1	0.2093	0.4724	0.5024	0.6848	1	0.6848	0.5027	0.4892
X_1X_4	0.4323	1	0.4323	0.9758	0.3389	0.2783	1	0.2783	0.2043	0.6578
X_2X_3	0.3511	1	0.3511	0.7924	0.3874	0.5006	1	0.5006	0.3675	0.5535
X_2X_4	114.65	1	114.65	258.78	<0.0001	105.94	1	105.94	77.77	<0.0001
X_3X_4	0.3278	1	0.3278	0.7398	0.4033	0.4727	1	0.4727	0.347	0.5646
X_1^2	1.83	1	1.83	4.13	0.0603	0.1223	1	0.1223	0.0898	0.7686
X_2^2	0.3517	1	0.3517	0.7937	0.387	0.3582	1	0.3582	0.2629	0.6156
X_3^2	1.48	1	1.48	3.33	0.0879	1.83	1	1.83	1.34	0.265
X_4^2	0.8231	1	0.8231	1.86	0.193	0.1413	1	0.1413	0.1037	0.7519
Residual	6.65	15	0.443			20.43	15	1.36		
Lack of fit	5.68	10	0.5678	2.94	0.1231 not significant	17.78	10	1.78	3.35	0.0972 not significant
Pure error	0.9671	5	0.1934			Pure error	2.65	5	0.53091	
Total	408.02	29				Total	563.3	29		

df = degrees of freedom.

Table 5b
Analysis of variance for fit of phenol degradation efficiency for UV/FeT/O_3, solar/FeT/O_3 processes using CCD-RSM model

	UV/FeT/O_3	Solar/FeT/O_3
Standard deviation	0.665	1.17
Mean	91.81	81.81
R^2	0.9837	0.9637
Adjusted R^2	0.9685	0.9299
Predicted R^2	0.9164	0.8114

compromised light penetration thus counteracting the effect of increasing catalyst surface area [34].

3.4. Effect of reaction time

It is found that the degradation efficiency of phenol increases with reaction time. It was observed that phenol degradation efficiency increases with time at a given pH with an increase in ozone concentration. It was observed that at basic pH phenol degradation efficiency decreases with the time at constant catalyst and ozone concentration. It was observed that there was no significant reduction in degradation efficiency after 30 min. As the reaction time increases beyond 30 min, there was very little further phenol removed as >90% of phenol had been degraded.

3.5. Optimization of process parameter

To obtain optimum condition the desired goal for phenol degradation efficiency was set as "maximize" while other independent parameters were set as "within the range". The phenol degradation efficiencies of 95.73% for the UV process and 86.46% for solar photocatalytic ozonation were obtained at the optimum condition of ozone concentration of 70 mg L^{-1}, catalyst concentration of 0.5 g L^{-1} at pH 10 and 20 min reaction time using RSM. The predicted results were validated by repeating experiments three times at optimum conditions and results indicated average phenol degradation efficiency. Table 7 shows the optimum condition for UV and solar systems. It can be concluded that the developed CCD-RSM model could be used effectively to optimize/study phenol degradation using the UV and solar photocatalytic ozonation process. Table 8 shows the comparison of the data of the present work with other published work.

Table 6
Values of regression coefficient of coded and actual factors for UV/FeT/O_3, solar/FeT/O_3 processes

Parameter	UV/FeT/O_3		Solar/FeT/O_3	
	Coded coefficient	Actual factors	Coded coefficient	Actual factors
Intercept	91.19	116.648	81.40	95.247
X_1-Ozone concentration	0.2262	–0.1534	0.295	0.0222
X_2-pH	–2.05	–3.2833	–2.184	–3.5581
X_3-Catalyst concentration	–0.2087	–8.415	0.0554	–3.3483
X_4-Reaction time	2.73	–1.1181	3.6262	–0.5680
X_1X_2	–0.0869	–0.0019	0.2093	0.0046
X_1X_3	0.1144	0.0305	–0.2068	–0.05517
X_1X_4	0.1644	0.00219	–0.1318	–0.00176
X_2X_3	–0.1481	–0.1975	–0.1768	–0.2358
X_2X_4	2.68	0.1784	2.573	0.1715
X_3X_4	0.1431	0.1145	0.1718	0.1375
X_1^2	0.2582	0.00115	0.0667	0.00029
X_2^2	0.1132	0.01258	0.1142	0.01269
X_3^2	0.232	3.71167	0.258	4.128
X_4^2	0.1732	0.00693	0.0717	0.00287

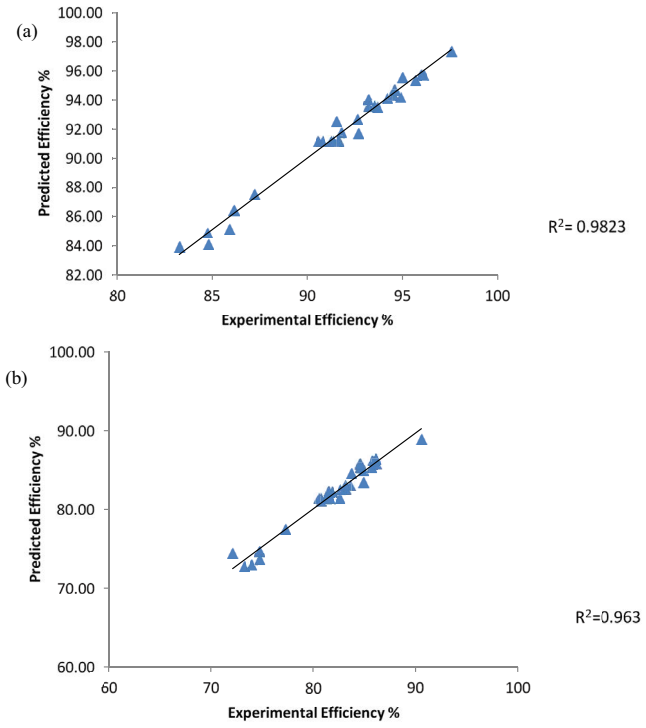

Fig. 6. Comparison of experimental and predicted phenol degradation efficiency using RSM: (a) UV/FeT/O_3 and (b) solar/FeT/O_3.

3.6. Synergy index

Synergism between TiO_2 photocatalysis and ozonation was observed for TOC and phenolic compound removal [37]. Ozone produces $OH^{\bullet}$ radicals on the FeT catalyst surface through the generation of the ozonide radical ion ($O_3^{\bullet-}$) during photocatalytic ozonation. Also, $OH^{\bullet}$ radicals were generated by ozone reaction with the superoxide ion radical and/or ozone photolysis [25]. Due to the competent trapping of photo-generated electrons by ozone, the recombination rate of electrons and holes was diminished which resulted in synergy.

The synergy index (SI) of photocatalytic ozonation was calculated using Eq. (15):

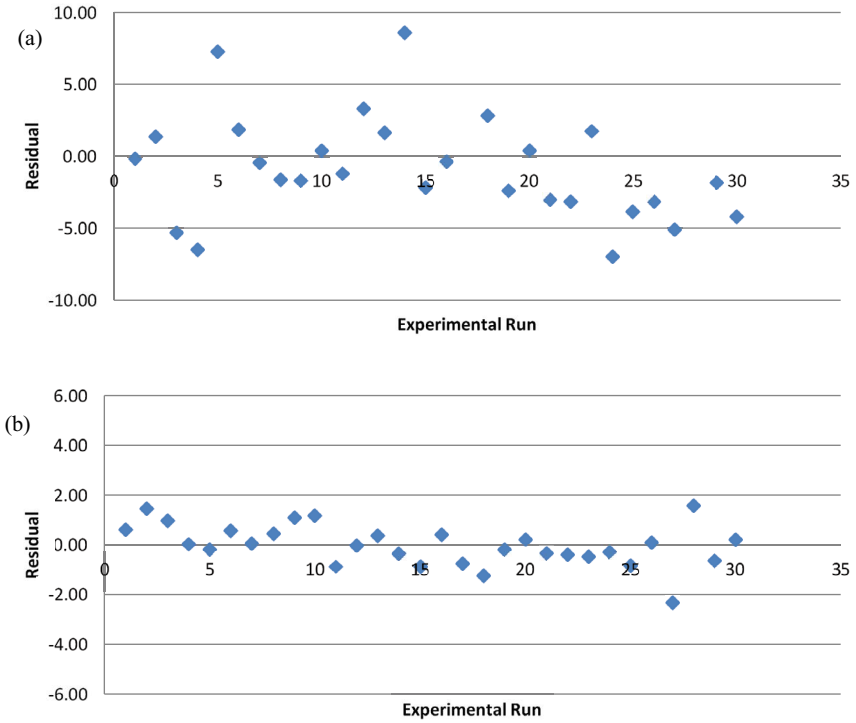

Fig. 7. Distribution of residuals for RSM: (a) UV/FeT/O_3 and (b) solar/FeT/O_3.

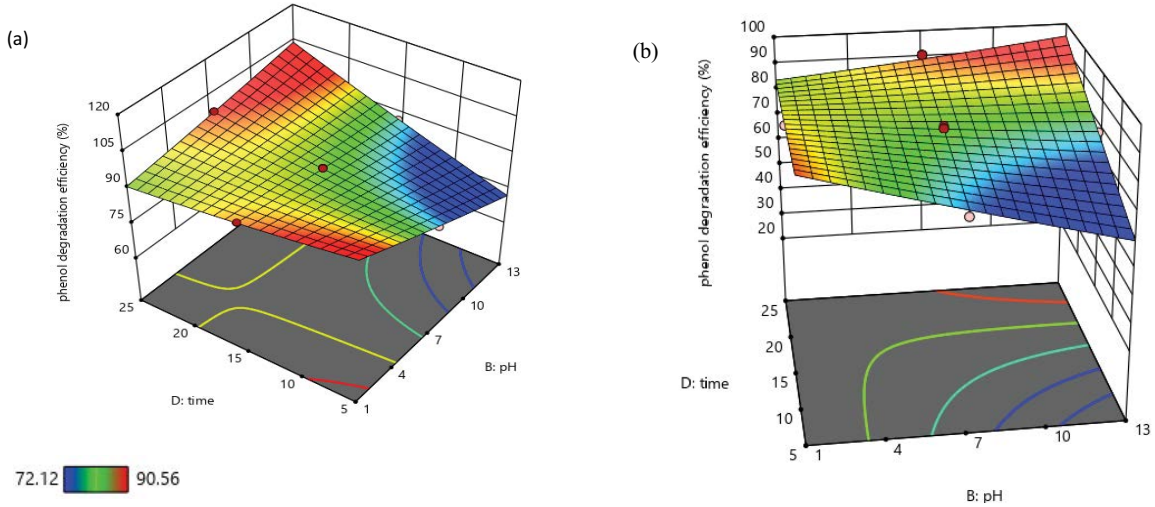

Fig. 8. Response surfaces for phenol degradation process as function of pH and reaction time: (a) UV/FeT/O_3 and (b) solar/FeT/O_3.

$$SI = \frac{R_{phot} + OZ}{R_{phot} + R_{OZ}} \quad (15)$$

where R is percentage phenol degradation efficiency, and subscript phot, OZ, and phot + OZ represent photocatalysis, ozonation, and combined photocatalysis ozonation, respectively. SI > 1 indicated that the combined process has a positive synergistic effect while SI < 1 denotes a negative effect.

The relative COD profiles are shown in Fig. 12 and the synergy index and the COD removal efficiencies are summarized in Table 9. The mineralization efficiencies were higher in both UV and solar photocatalytic ozonation than in ozonation and photocatalytic oxidation alone. Synergy index values of 1.02–1.25 were obtained between ozonation and photocatalysis using solar and UV photocatalytic ozonation. The synergy between ozonation and photocatalysis reduced the reaction time by increasing the reaction rate constants thereby reducing energy requirement for the combined processes [25]. This may be due to the increased production of $OH^{\bullet}$ radicals which enhanced the degradation of pollutants.

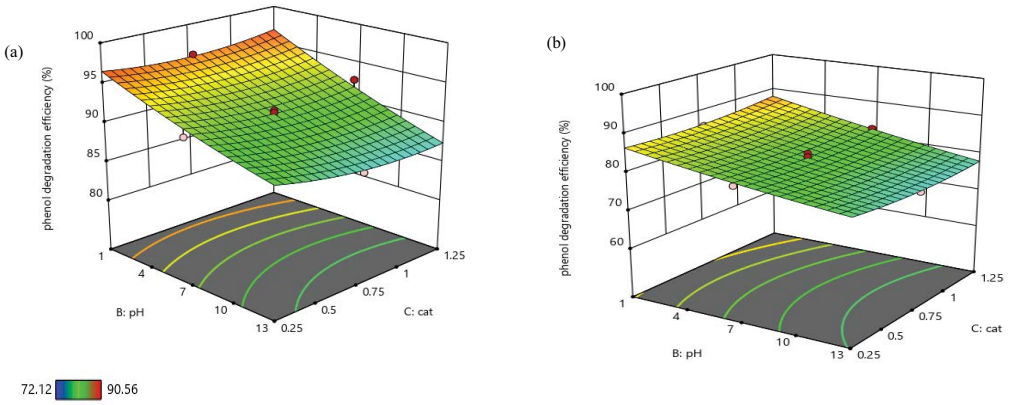

Fig. 9. Response surfaces for phenol degradation process as function of catalyst concentration and pH: (a) UV/FeT/O_3 and (b) solar/FeT/O_3.

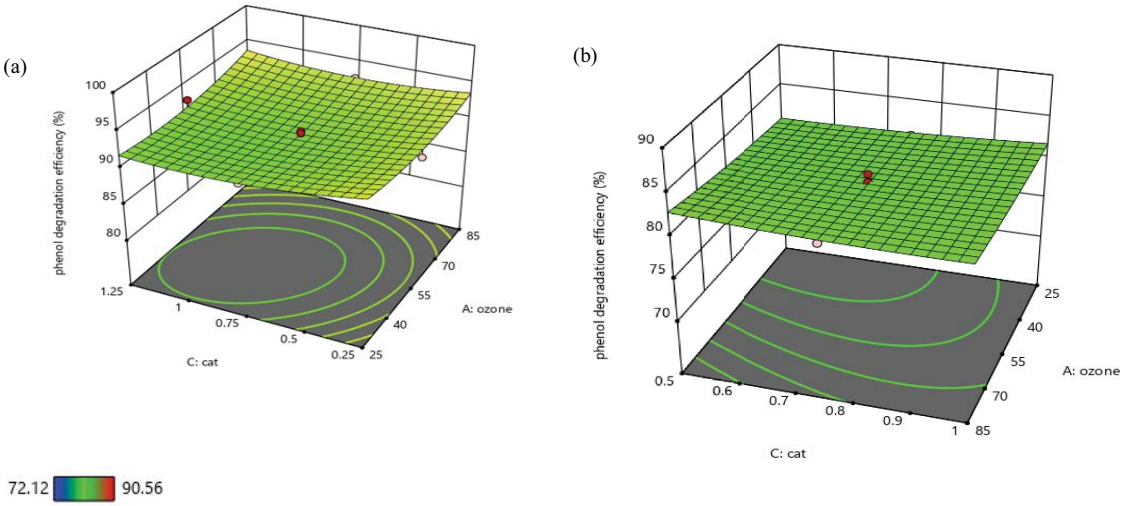

Fig. 10. Response surfaces for phenol degradation process as function of catalyst concentration and ozone concentration: (a) UV/FeT/O_3 and (b) solar/FeT/O_3.

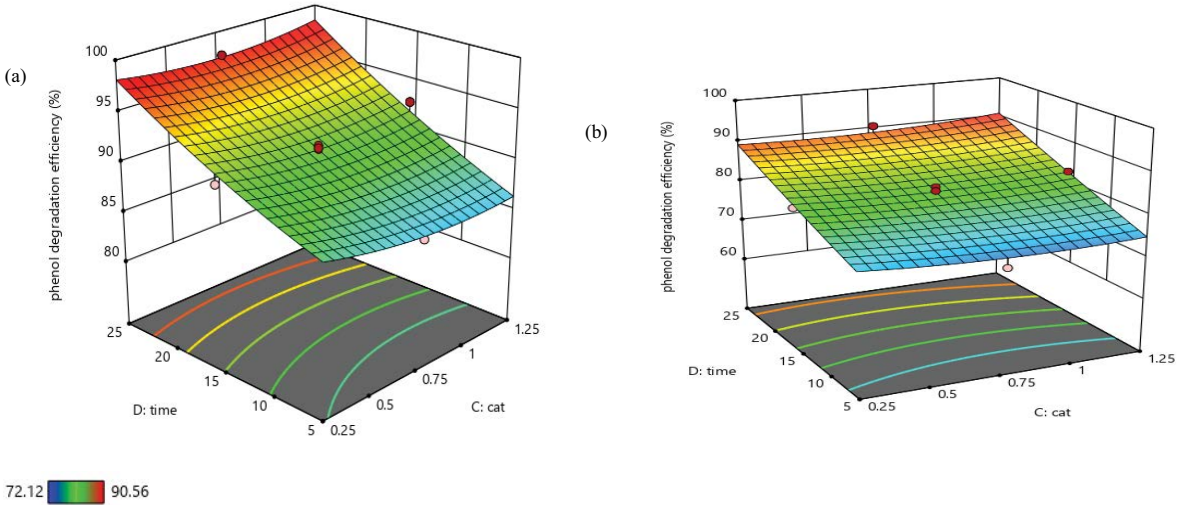

Fig. 11. Response surfaces for phenol degradation process as function of catalyst concentration and reaction time: (a) UV/FeT/O_3 and (b) solar/FeT/O_3.

Table 7
Comparison of the experimental and predicted value of optimum phenol degradation efficiency for UV/FeT/O_3, solar/FeT/O_3 processes using CCD-RSM

	Optimum value predicted		Experimental value	
Variable	UV/FeT/O_3	Solar/FeT/O_3	UV/FeT/O_3	Solar/FeT/O_3
Ozone concentration (mg L^{-1})	70	70	70	70
Initial pH	10	10	10	10
Catalyst concentration (g L^{-1})	0.5	0.5	0.5	0.5
Reaction time (min)	20	20	20	20
Phenol degradation efficiency (%)	95.73	86.46	96.12	86.12

Table 8
Comparison of the data of present work with other published work

System	Optimum conditions					Degradation efficiency (%)	Reference
	Ozone concentration (mg L^{-1})	Catalyst concentration (mg L^{-1})	pH	Reaction time (min)	Phenol concentration (mg L^{-1})		
UV/FeT/O_3	20.83	0.5	6	120	50	99.3	[25]
UV/FeT/O_3	70	0.5	10	20	500	96.12	Present study
Solar/FeT/O_3	20.83	0.5	6	60	5	69	[25]
Solar/FeT/O_3	70	0.5	10	20	500	86.12	Present study

Table 9
COD removal efficiencies (R) and SI for UV and solar photocatalytic ozonation (500 mg L^{-1} phenol concentration; O_3 concentration 70 mg L^{-1}; pH 10; 0.5 g L^{-1} catalyst concentration; 20 min)

Process	R	SI	Process	R	SI
O_3	26.34	–	O_3	26.34	–
UV/FeT	44.47	–	Solar/FeT	30.88	–
UV/FeT/O_3	88.00	1.25	Solar/FeT/O_3	57.02	1.02

3.7. Kinetics

The mechanism of phenol ozonation consisted of a complex pathway of substitution and cycloaddition reaction and the ratio of the concentration of the dissociated and non-dissociated form of phenol varies with pH and with reactivity with ozone. The reacting system depended on mass transfer associated with the kinetic regime of ozone absorption as well as UV radiation [38]. The mass transfer depended on pH, composition, gas flow rate, ozone concentration, bubble size, etc. [39]. Owing to the low solubility of ozone into the water, the mass transfer of ozone was the rate-limiting step in the ozonation of phenol. When ozone inlet concentration exceeds a critical value, the rate-limiting step would turn into a kinetically controlled regime [40]. The previous studies [13,14,25,41] using UV and solar photocatalytic ozonation confirmed the applicability of the pseudo-first-order kinetic model. By plotting $\ln(C_0/C_t)$ against time (Fig. 13), the apparent rate constant can be determined from the slope of the line. The apparent rate constant was found to be 0.084 min^{-1}, with a correlation coefficient of 0.964 indicating goodness of fit. The apparent first-order rate constant was an approximately linear function of dissolved ozone concentration [42]. Benzoquinone, catechol, hydroquinone, and oxalic acid intermediate products occur at the end of phenol ozonation while small organic acids, CO_2, and H_2O are major final products during phenol ozonation [7,43].

3.8. Treatment of municipal wastewater

The UV and solar photocatalytic ozonation for the degradation of phenol in synthetic solution have been studied in the preceding section while the objective of the present study is to investigate the photocatalytic ozonation of secondary municipal wastewater using FeT catalyst. The phenol concentration in secondary municipal wastewater was set at 500 mg L^{-1} which was much higher than the typical phenol concentration (500–5,000 μg L^{-1}) in municipal wastewater in India [44] was chosen to determine the robustness of the treatment process. The optimum COD removal efficiency for UV and solar photocatalytic ozonation of SWW is summarized in Table 10. It was observed that the COD removal efficiencies are higher under UV radiation. This may be due to differences in light intensities used. It was found that there is a decrease in the COD for both UV/FeT/O_3 and solar/FeT/O_3 processes. The final COD values for both UV and solar processes met the guidelines for wastewater discharge in India (COD < 30 mg L^{-1}). It can be concluded that photocatalytic ozonation was efficient in reducing recalcitrant pollutants to meet the set standard for wastewater discharge (COD). However, further tests on microbiological

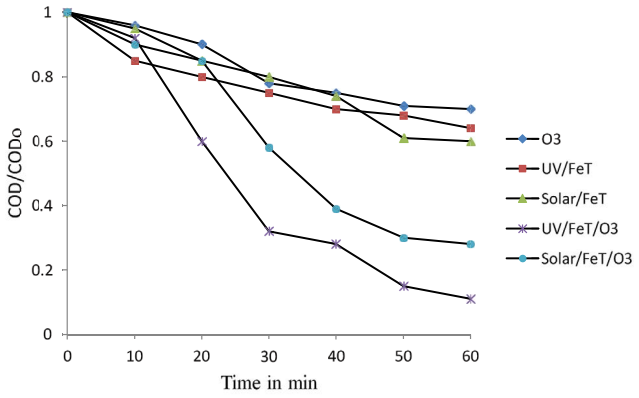

Fig. 12. COD profile for phenol degradation using ozonation, photocatalytic oxidation, photocatalytic ozonation (500 mg L^{-1} phenol concentration; O_3 concentration 70 mg L^{-1}; pH 10; 0.5 g L^{-1} catalyst concentration).

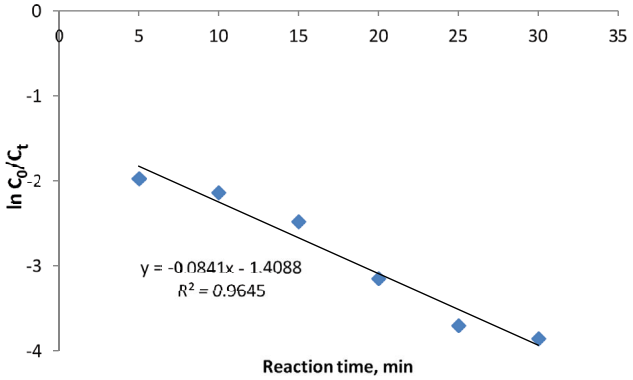

Fig. 13. Phenol degradation kinetics for photocatalytic ozonation process.

Table 10
Summary of COD degradation efficiencies of SWW after photocatalytic ozonation treatment

Process	COD removal efficiency (%)
UV/FeT/O_3	68.40
Solar/FeT/O_3	50.80

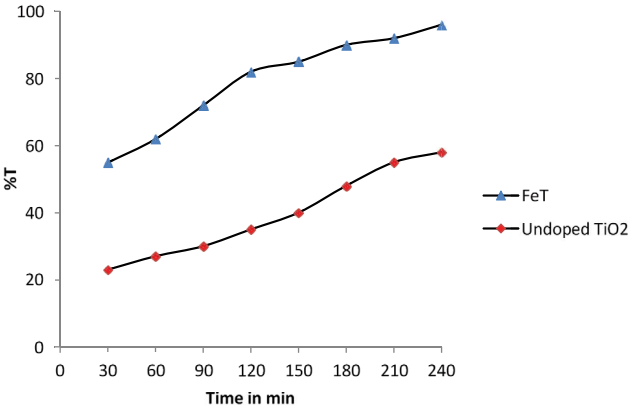

Fig. 14. Sedimentation rate profile.

quality and toxicity studies may be required to make water fit for human consumption [34]. It can be concluded from the literature that the toxicity of phenol water was reduced significantly during photocatalytic ozonation [27,28].

3.9. Sedimentation rate profile

It is difficult to separate fine catalyst nanoparticles after the degradation of pollutants. Although ultrasonic irradiation, coagulation, cross-flow microfiltration, and foam flotation method have been suggested [45], these methods require a specific separation process. The FeT nanoparticles were satisfactorily sedimented within 4 h (Fig. 14) and the turbidity of the supernatant solution was <1 NTU. Therefore, the FeT particle could be separated from wastewater by settling only because of their higher specific gravity than that of undoped TiO_2. Also, there is no need to add any coagulants or electrolytes to the reaction mixture.

3.10. Treatment efficiency

In process economics, the treatment cost based on electric energy consumption plays an important role. The optimum parameters obtained from RSM were analyzed for their treatment efficiency. The treatment cost and energy efficiency for each process were determined based on energy consumption to reduce the undesired components (COD in this case) as mentioned in studies of Nakhate et al. [46]:

The power dissipation per unit volume (power density) = maximum power required for ozonation unit for 20 min of treatment process = 216 W L^{-1}, that is, 259,200 J L^{-1}.

The energy efficiency is calculated as the amount of COD reduced per unit power dissipation.

Also, the energy required for COD reduction is calculated as the amount of initial COD per unit energy efficiency. In India, the cost for 1 kWh electricity differs according to the state and grid. Hence, by considering the cumulative 10 Rs/1 kW h cost of electricity, 2.73 Rs. was required to treat a 1 L sample using ozonation alone. Based on this calculation, the cost for other processes has been calculated as shown in Table 11. The treatment cost required based on power dissipation was found to be less in the case of the UV/FeT process, but the COD reduction capacity is found to be limited whilst, the COD reduction capacity was found to be better in UV/FeT/O_3 process despite the slightly high cost.

4. Conclusion

Photocatalytic ozonation using UV and solar light using Fe doped TiO_2 nanocatalyst were studied for the oxidation of phenol in synthetic water and actual secondary municipal wastewater. The phenol concentration employed is much higher than the typical phenol concentration in the environmental sample and thus exhibiting the robustness of the process. The study reveals that photocatalytic ozonation presents several advantages like high effectiveness,

Table 11
Comparison of treatment efficiency between various systems based on electric energy consumption

Process	COD removal efficiency	Power dissipation	Energy efficiency (mg L^{-1})	Energy required per unit volume (J L^{-1})	Energy required (kWh)	Total cost related to power (Rs L^{-1})
O_3	26.34	216	5.28×10^{-5}	9.848×10^{5}	0.273	2.73
UV/FeT	44.47	20	9.6×10^{-4}	5.41×10^{4}	0.015	0.15
UV/FeT/O_3	88.00	236	16.15×10^{-5}	3.21×10^{5}	0.089	0.89
Solar/FeT/O_3	57.02	216	1.145×10^{-4}	4.541×10^{5}	0.1261	1.26

low energy consumption, recovery of the photocatalyst, and detoxification of the wastewater, also leads to a reduction in capital cost due to the use of one reactor for simultaneous photocatalysis and ozonation instead of two separate reactors. The use of solar photocatalytic ozonation using FeT catalyst offers an economic advantage over costly commercial UV lamps. The use of solar radiation in photocatalytic ozonation makes the technology more cost-effective and competitive, especially an attractive process for wastewater in sunlight abundant countries like India.

References

[1] S.G. Ballesteros, M. Mora, R. Vicente, R.F. Vercher, C. Sabater, M.A Castillo, A.M. Amat, A. Arques, A new methodology to assess the performance of AOPs in complex samples: application to the degradation of phenolic compounds by O_3 and O_3/UV-A-Vis, Chemosphere, 222 (2019) 114–123.

[2] D.B. Silva, C.A. Alcalde, C. Sans, J. Giménez, S. Esplugas, Performance and kinetic modeling of photolytic and photocatalytic ozonation for enhanced micropollutants removal in municipal wastewaters, Appl. Catal., B, 249 (2019) 211–217.

[3] M. Farzadkia, D.Y. Shahamat, S. Nasseri, A.H. Mahvi, M. Gholami, A. Shahryari, Catalytic ozonation of phenolic wastewater: identification and toxicity of intermediates, J. Eng., 2014 (2014) 1–10.

[4] D.A. Piña, G.R. Morales, C.B. Díaz, P.B. Hernandez, E.M. Campo, R. Natividad, Synergic effect of ozonation and electrochemical methods on oxidation and toxicity reduction: phenol degradation, Fuel, 198 (2017) 82–90.

[5] Y. Xie, Y. Chen, J. Yang, C. Liu, H. Zhao, H. Cao, Distinct synergetic effects in the ozone enhanced photocatalytic degradation of phenol and oxalic acid with Fe^{3+}/TiO_2 catalyst, Chin. J. Chem. Eng., 26 (2018) 1528–1535.

[6] M. Mehrjouei, S. Müller, D. Möller, A review on photocatalytic ozonation used for the treatment of water and wastewater, Chem. Eng. J., 263 (2015) 209–219.

[7] K. Turhan, S. Uzman, Removal of phenol from water using ozone, Desalination, 229 (2008) 257–263.

[8] S. Mohammadi, A. Kargari, H. Sanaeepur, K. Abbassian, A. Najafi, E. Mofarrah, Phenol removal from industrial wastewaters: a short review, Desal. Water Treat., 53 (2014) 2215–2234.

[9] L.G.C. Villegas, N. Mashhadi, M. Chen, D. Mukherjee, K.E. Taylor, N. Biswas, A short review of techniques for phenol removal from wastewater, Curr. Pollut. Rep., 2 (2016) 157–167.

[10] T. Ali, P. Tripathi, A. Azam, W. Raza, A.S. Ahmed, A. Ahmed, M. Muneer, Photocatalytic performance of Fe-doped TiO_2 nanoparticles under visible-light irradiation, Mater. Res. Express, 4 (2017) 015022, doi: 10.1088/2053-1591/aa576d.

[11] M.V. Swapna, K.R. Haridas, An easier method of preparation of mesoporous anatase TiO_2 nanoparticles via ultrasonic irradiation, J. Exp. Nanosci., 11 (2016) 540–549.

[12] M.M. Viana, V.F. Soares, N.D.S. Mohallem, Synthesis and characterization of TiO_2 nanoparticles, Ceram. Int., 36 (2010) 2047–2053.

[13] S. Bhattacharjee, S. Chakraborty, K. Mandol, L. Liu, H. Choi, C. Bhattacharjee, Optimization of process parameters during photocatalytic degradation of phenol in UV annular reactor, Desal. Water Treat., 54 (2015) 2270–2279.

[14] A.C. Mecha, M.S. Onyango, A. Ochieng, T.S. Jamil, C.J.S. Fourie, M.N.B. Momba, UV and solar light photocatalytic removal of organic contaminants in municipal wastewater, Sep. Sci. Technol., 51 (2016) 1765–1778.

[15] K. Salehi, B. Shahmoradi, A. Bahmani, M. Pirsaheb, H.P. Shivaraju, Optimization of reactive Black 5 degradation using hydrothermally synthesized NiO/TiO_2 nanocomposite under natural sunlight irradiation, Desal. Water Treat., 57 (2016) 25256–25266.

[16] S. Amirkhanloun, M. Ketabchi, N. Parvin, Nanocrystalline/nanoparticles ZnO synthesized by high energy ball milling process, Mater. Lett., 86 (2012) 122–124.

[17] S.B. Eadi, S. Kim, S.W. Jeong, H.W. Jeon, Novel preparation of Fe doped TiO_2 nanoparticles and their application for gas sensor and photocatalytic degradation, Adv. Mater. Sci. Eng., 2017 (2017) 1–6.

[18] M.B. Marami, M. Farahmandjou, B. Khoshnevisan, Sol–gel synthesis of Fe-doped TiO_2 nanocrystals, J. Electron. Mater., 47 (2018) 3741–3748.

[19] I. Ganesh, P.K. Polkampally, A.K. Gupta, P.S.C. Sekhar, K. Radha, G. Padmanabham, G. Sundararajan, Preparation and characterization of Fe-doped TiO_2 powders for solar light response and photocatalytic applications, Process. Appl. Ceram., 6 (2012) 21–36.

[20] A. Kerrami, L. Mahtout, F. Bensouici, M. Bououdina, S. Rabhi, E. Sakher, H. Belkacemi, Synergistic effect of rutile-anatase Fe-doped TiO_2 as efficient nanocatalyst for the degradation of Azucryl Red, Mater. Res. Express, 6 (2019) 0850f5, doi: 10.1088/2053-1591/ab2677.

[21] S. Sood, A. Umarb, S.K. Mehta, S.K. Kansal, Highly effective Fe-doped TiO_2 nanoparticles photocatalysts for visible-light driven photocatalytic degradation of toxic organic compounds, J. Colloid Interface Sci., 450 (2015) 213–223.

[22] C.L. Luu, Q.T. Nguyen, S.T. Ho, Synthesis and characterization of Fe-doped TiO_2 photocatalyst by the sol–gel method, Adv. Nat. Sci. Nanosci. Nanotechnol., 1 (2010) 015008, doi: 10.1088/2043-6254/1/1/015008.

[23] D.H. Quiñones, P.M. Álvarez, A. Rey, F.J. Beltrán, Removal of emerging contaminants from municipal WWTP secondary effluents by solar photocatalytic ozonation: a pilot-scale study, Sep. Purif. Technol., 149 (2015) 132–139.

[24] A. Espejo, F.J. Beltrán, F.J. Rivas, J.F. García-Araya, O. Gimeno, Iron based catalysts for photocatalytic ozonation of some emerging pollutants of wastewater, J. Environ. Sci. Health Part A, 50 (2015) 553–562.

[25] A.C. Mecha, M.S. Onyango, A. Ochieng, C.J.S. Fourie, M.N.B. Momba, Synergistic effect of UV-vis and solar photocatalytic ozonation on the degradation of phenol in municipal wastewater: a comparative study, J. Catal., 341 (2016) 116–125.

[26] J. Xiao, Y. Xie, H. Cao, Organic pollutants removal in wastewater by heterogeneous photocatalytic ozonation, Chemosphere, 121 (2015) 1–17.

[27] C. Mecha, M.S. Onyango, A. Ochieng, M.N.B. Momba, Evaluation of synergy and bacterial re-growth in photocatalytic

ozonation disinfection of municipal wastewater, Sci. Total Environ., 601–602 (2017) 626–635.
[28] A.C. Mecha, M.S. Onyango, A. Ochieng, M.N.B. Momba, Ultraviolet and solar photocatalytic ozonation of municipal wastewater: catalyst reuse, energy requirements and toxicity assessment, Chemosphere, 186 (2017) 669–676.
[29] M. Ghorbanpour, A. Feizi, Iron-doped TiO_2 catalysts with photocatalytic activity, J. Water Environ. Nanotechnol., 4 (2019) 60–66.
[30] M. Taghavi, M.T. Ghaneian, M.H. Ehrampoush, M. Tabatabaee, M. Afsharnia, A. Alami, J. Mardaneh, Feasibility of applying the LED-UV-induced TiO_2/ZnO-supported $H_3PMo_{12}O_{40}$ nanoparticles in photocatalytic degradation of aniline, Environ. Monit. Assess., 190 (2018) 188, doi: 10.1007/s10661-018-6565-y.
[31] N. Marchitan, C. Cojocaru, A. Mercuta, G. Gupta, I. Cretescu, M. Gonta, Modeling and optimization of tartaric acid reactive extraction from aqueous solution: a comparison between response surface methodology and artificial neural network, Sep. Purif. Technol., 75 (2010) 273–285.
[32] F. Geyikei, E. Kilic, S. Coruh, S. Elevli, Modeling of lead adsorption from industrial sludge leachate on the red mud by using RSM and ANN, Chem. Eng. J., 183 (2012) 53–59.
[33] J. Hoigné, H. Bader, Rate constants of reactions of ozone with organic and inorganic compounds in water-II. Dissociating organic compounds, Water Res., 17 (1983) 185–194.
[34] C.V. Rekhate, J.K. Srivastava, Recent advances in ozone-based advanced oxidation processes for treatment of wastewater - a review, Chem. Eng. J. Adv., 3 (2020) 100031, doi: 10.1016/j.ceja.2020.100031.
[35] A.C. Mecha, M.S. Onyango, A. Ochieng, M.N.B. Momba, Impact of ozonation in removing organic micro-pollutants in primary and secondary municipal wastewater: effect of process parameters, Water Sci. Technol., 74 (2016) 756–765.
[36] Z. Zeng, H. Zou, X. Li, M. Arowo, B. Sun, J. Chen, G. Chu, L. Shao, Degradation of phenol by ozone in the presence of Fenton reagent in a rotating packed bed, Chem. Eng. J., 229 (2013) 404–411.
[37] M.M. Rodríguez, G. Márquez, E.A. León, P.M. Álvarez, A.M. Amat, F.J. Beltrán, Mechanism considerations for photocatalytic oxidation, ozonation and photocatalytic ozonation of some pharmaceutical compounds in water, J. Environ. Manage., 127 (2013) 114–124.
[38] T. Poznyak, J. Vivero, Degradation of aqueous phenol and chlorinated phenols by ozone, Ozone Sci. Eng., 27 (2005) 447–458.
[39] L.L.C. Catorceno, K.R.B. Nogueira, A.C.S.C. Teixeira, Treatment of aqueous effluents containing phenol by the O_3, O_3-UV, and O_3-H_2O_2 processes: experimental study and neural network modeling, Sep. Sci. Technol., 45 (2010) 1521–1528.
[40] W. Cheng, X. Quan, R. Li, J. Wu, Q. Zhao, Ozonation of phenol-containing wastewater using O_3/$Ca(OH)_2$ system in a micro bubble gas-liquid reactor, Ozone Sci. Eng., 40 (2017) 173–182.
[41] W. Pratarn, T. Pornsiri, S. Thanit, C. Tawatchai, T. Wiwut, Adsorption and ozonation kinetic model for phenolic wastewater treatment: catalysis, kinetics and reactors, Chin. J. Chem. Eng., 19 (2011) 76–82.
[42] K. Muroyama, S. Suwa, A. Kawabata, Y. Takami, J. Hayashi, Effects of addition of hydrogen peroxide and/or calcium carbonate on ozone-decomposition of phenol sparingly dissolved in water, Ozone Sci. Eng., 33 (2011) 143–149.
[43] M.K. Ramseier, U. Gunten, Mechanisms of phenol ozonation—kinetics of formation of primary and secondary reaction products, Ozone Sci. Eng., 31 (2009) 201–215.
[44] Environmental Standards for Ambient Air, Automobiles, Fuel, Industries and Noise, Central Pollution Control Board, India. Available at: http://www.cpcbenvis.nic.in/
[45] S. Nahar, K. Hasegawa, S. Kagaya, Photocatalytic degradation of phenol by visible light-responsive iron-doped TiO_2 and spontaneous sedimentation of the TiO_2 particles, Chemosphere, 65 (2006) 1976–1982.
[46] P.H. Nakhate, H.G. Patil, K.V. Marathe, Intensification of landfill leachate treatment by advanced Fenton process using classical and statistical approach, Chem. Eng. Process. Process Intensif., 133 (2018) 148–159.